Micromechanical Studies of Strain Rate Dependent Compressive Strength in Brittle Polycrystalline Materials

Hao Jiang, Zongyue Fan and *†Bo Li

Department of Mechanical and Aerospace Engineering, Case Western Reserve University, Cleveland, OH 44106, USA.

*Presenting author: bxl295@case.edu
†Corresponding author: bxl295@case.edu

Abstract

We propose a micromechanical computational framework for the high fidelity prediction of failure mechanisms in brittle polycrystalline materials. A three-dimensional direct numerical simulation of polycrystalline structures is constructed to explicitly account for the microstructural features, such as grain sizes, grain orientations, and grain boundary misorientations, by using the finite element method. In particular, grain boundaries are represented by a thin layer of elements with non-zero misorientation angles. The Eigen-fracture algorithm is employed to predict the crack propagation in the grain structure including intergranular and transgranular fractures. In the Eigen-fracture approach, an equivalent energy release rate is defined at the finite elements to evaluate the local failure state by comparing to the critical energy release rate, which varies at the grain boundaries and the interior of grains. Moreover, the constitutive model is considered as functions of the local microstructure features. As a result, the anisotropic response of brittle polycrystalline materials and the interaction between the fracture and topological defects in the microstructure under general loading conditions are explicitly modeled. Finally, the compressive dynamic response of hexagonal SiC with equiaxed grain structures is studied at different strain rates by using the proposed computational framework. The predicted compressive strength as well as the strain rate dependence of SiC agrees well with measurements in Split Hopkins Pressure Bar (SHPB) experiments.

Keywords: Brittle fracture Polycrystalline; Eigen-fracture; Anisotropic; Dynamic compression; Grain boundary

Introduction

Modern structural ceramics and ceramic composites have been considered as high-performance materials due to the high-temperature stability, high hardness, low density and superior elastic moduli and strength. These exceptional thermal and mechanical properties in ceramics lead to a wide range of applications, such as lightweight armors for personal protection and high performance turbine blades. Nevertheless, unlike metal or polymers, the failure of ceramics is usually sudden and catastrophic. This feature in failure mechanisms of brittle polycrystalline materials including monolithic ceramics and ceramic composites makes it challenging to accurately predict their resistance to extreme loading conditions, especially impact loading at high strain rates. In addition, the ultimate strength of ceramic has been observed to be strain-rate sensitive ([1]–[4]). While it has been generally recognized that the rate-dependent behavior is related to the intrinsic microstructures and flaws (e.g., crystal structure, grain orientation, grain boundaries, micro-voids, second phase particle and stacking faults), evolution of the microstructure, in particular, dynamic interaction between the crack and topological defects in the microstructure, at high strain rates has not been addressed quantitatively due to the lack of fundamental understanding and the limitations in experimental diagnostics. Sarva and Nasser

studied strain rate sensitivity of Silicon Carbide under compression[1]. They found that, beside of the compressive strength, the fragment sizes are also rate sensitive. Smaller fragment sizes were obtained at higher strain rates, which indicates more micro-cracks took place. Wang and Ramesh performed experimental studies on hot-pressed SiC under high strain rate compression in 2004 [2]. By analyzing the failure process, their results show that the subcritical micro crack propagates and coalesces before macro crack splits. Recent studies on the dynamic behavior of AlN ([3], [4]) indicates that transgranular fracture becomes more common at high strain rates. Chan and Ravichandran performed similar studies on AlN [5], which show that ceramics exhibit an increase in shear strength with increasing confinement pressure and a strain-rate-sensitive material model was developed with fitting to experimental data. To date, the experimental investigations listed in the above literature and others characterize the rate-dependent dynamic response of brittle polycrystalline materials at the macro-scale. However, the underlying micromechanisms are only perceived in a qualitative manner. There is very few, if any, quantitative analysis at the microstructure level to explain the rate sensitivity of the compressive strength in brittle materials by experiments.

Alternatively, computational models and numerical simulations have been utilized to predict the strain rate dependent failure mechanisms in brittle materials. The wing-crack array model ([1], [2], [6]) is commonly adopted to explain the mechanism of strain rate effect. The wing-crack array model utilizes the local stress intensity at the preexisting crack as the failure criterion. The rate-dependent influence is included by considering inertia effects at the crack tip. The final strength of the material is related to the initial flaw size and the flaw distribution. However, rate-dependent material coefficients are introduced in the model and need to be calibrated to experiments. On the other hand, topological defects in the microstructure, such as grain boundaries and grain orientations are not explicitly accounted for. The intergranular fractures are often modeled using a cohesive surface approach within finite element formulation ([7]–[10]).The cohesive method provides a phenomenological framework to describe the traction–displacement relation of the crack surface. The fracture characteristics and anisotropic properties of the grain boundaries are embedded in the cohesive elements. When the crack surfaces are fully separated, a contact algorithm can be employed to deal with the friction between fractured interfaces. Similar to wing crack model, an intrinsic flaw length is introduced into the model. In addition, a characteristic relaxation time is derived to explain the rate dependent character of the failure strength ([11], [12]). Nittur and others[9] investigated the dynamic fragmentation of ceramic under compression. They have found that the material remains largely intact when peak compressive strength is achieved, but shows a catastrophic increase in accumulated damage after that point. Sfantos and Aliabadi[10] also studied the intergranular fracture in brittle material under compression. They found that the internal friction of the material becomes important in cases of compressive localized pressures over cracked surfaces. As this internal friction increases, crack propagation was slowed down while crack branching appeared faster. For most polycrystalline related cohesive models, only the intergranular fracture is included ([7]–[10]). It is computationally consuming for modeling transgranular fracture since each element surface/edge require a cohesive element. The fracture path is constrained to follow element interfaces that rely on the mesh spacing and orientation. It has been stated out that the cohesive zone models suffer from mesh-dependence and the lack of strict conservation and convergence properties [13]. Most recently, the phase field model becomes popular to simulate the fracture process ([14]–[16]) In this method, the discontinuities caused by crack is approximated by a phase-field. The phase field is independent of the displacement field and can be calculated implicitly. An order parameter is introduced along the crack to accommodate the material transition from the undamaged to the damaged state. The phase field model for quasi-static brittle fracture can be derived from the variational formulation

for Griffith's type of fracture models [17]. Therefore, less user-defined parameters and fracture criteria are required. However, the material properties of the damaged material need to be estimated and the order parameter function through the fracture thickness needs to be calibrated. The polycrystalline phase field model developed by Clayton and Knap is able to capture the changes of crack paths and bulk material properties by changing the grain boundary properties. However, to predict the strain rate sensitivity in the dynamic response of brittle materials, rate-dependent phase field model needs to be further developed.

Another variational approach to fracture is deducted using Eigen-fracture scheme based on element erosion ([18],[19]). Similar to phase field model, the discontinuities are approximated using an Eigen-deformation field, which is widely used in mechanics to describe deformation modes that cost no local energy. Instead of considering the energy minimization globally by the phase field method, the Eigen-fracture approach regards fracture as a dissipative process with dissipation located at the crack front [20]. In this approach, the crack front velocity obeys a kinetic law in terms of the local driving force, and the entire trajectories of the system, including the crack paths, follow as minimizers of energy-dissipation functional [21]. In this regard, the propagation of the crack can be related to the combination and competition of various energy dissipation pathways in the materials microstructure. Different types of defects, preexisting micro cracks, grain boundaries and etc., can all be considered as potential energy sinks to minimize energy when stress flow passing by.

In this work, a micromechanical computational framework based on the Eigen-fracture scheme is presented for the high fidelity prediction of failure mechanisms in brittle polycrystalline materials. A direct numerical simulation of the polycrystalline structure explicitly accounts for the microstructural features, such as grain sizes, grain orientations, and grain boundary misorientations, by using the finite element method. Furthermore, it furnishes an effective manner to directly accommodate other types of defects, including porosity and second phase particles. An equivalent energy release rate is defined at the finite elements to evaluate the local failure state by comparing to the critical energy release rate, which varies at the grain boundaries and the interior of grains. Since the calculation of the equivalent energy release rate is carried out within a local neighborhood of an element, it has the effect of eliminating spurious mesh-dependent artifacts. The Eigen-fracture scheme is known to properly converge to Griffith fracture in the limit of vanishingly small mesh sizes. The anisotropic characters of the polycrystalline structure are obtained by using a crystal elasticity constitutive model and grain boundary properties related to the misorientation angles. In order to validate the proposed computational framework, the compressive dynamic response of hexagonal SiC with equiaxed grain structures is studied numerically at different strain rates and compared to experimental measurements.

General Framework

In this section, the general framework for analyzing the brittle polycrystalline material response at the grain scale will be presented based on the finite element method. Since this work focuses on the crack propagation in the polycrystalline microstructure (6H SiC in particular), the crystal elasticity model is integrated to describe the anisotropic constitutive relationship ([22], [23]). The study of failure mechanisms is carried out by using the Eigen-fracture model ([18], [24]), which is an energy-based variational fracture principle to the generalized Griffith's model.

Governing equations

Given initial and boundary conditions, the dynamic deformation problem can be analyzed using finite element method by seeking solutions of the governing equations of conservation of mass

and momentum. Consider a body initially occupying a reference configuration Ω_0 in a d-dimensional Euclidean space with boundary Γ. Suppose the boundary can be decomposed into the essential boundary Γ_u and natural boundary Γ_t, such that $\Gamma = \Gamma_u \cup \Gamma_t$ and $\Gamma_u \cap \Gamma_t = \emptyset$. The differential form of conservation equations can be written, respectively, in the Lagrangian configuration as

$$\rho = \frac{\rho_0}{J} \text{ in } \Omega_0, \tag{1}$$

$$\nabla \cdot \boldsymbol{P} + \rho_0 \boldsymbol{B} = \rho_0 \boldsymbol{A} \qquad \text{in } \Omega_0, \tag{2}$$

where ρ_0 and ρ are the density in the reference and deformed configuration, respectively, $\boldsymbol{F}$ the deformation gradient, J the Jacobian defined as $J = \det(\boldsymbol{F})$, $\boldsymbol{P}$ the first Piola-Kirchhoff stress tensor, $\boldsymbol{B}$ the body force density per unit undeformed volume and $\boldsymbol{A}$ the acceleration. The first Piola-Kirchhoff stress tensor $\boldsymbol{P}$ and the Cauchy stress tensor $\boldsymbol{\sigma}$ is related as

$$\boldsymbol{P} = J\boldsymbol{\sigma}\boldsymbol{F}^{-T}, \tag{3}$$

The essential and natural boundary conditions are given by

$$\boldsymbol{u} = \bar{\boldsymbol{u}} \qquad \text{on } \Gamma_u, \tag{4}$$

$$\boldsymbol{P} \cdot \boldsymbol{N} = \bar{\boldsymbol{t}} \quad \text{on } \Gamma_t, \tag{5}$$

where $\bar{\boldsymbol{u}}, \bar{\boldsymbol{t}}$ and $\boldsymbol{N}$ are the prescribed displacement on the essential boundary, the external traction on the natural boundary and the unit outward normal to Γ_t, respectively. The displacement is denoted by $\boldsymbol{u}$, which is related to the deformation gradient as

$$\boldsymbol{F} = \nabla \boldsymbol{u} + \mathbf{I}. \tag{6}$$

The weak form associated with the governing equations follows from the principle of virtual work as,

$$\int_{\Omega_0} [\boldsymbol{P} : \nabla(\delta \boldsymbol{u}) - \rho_0(\boldsymbol{B} - \boldsymbol{A}) \cdot \delta \boldsymbol{u}] dV - \int_{\Gamma_t} \bar{\boldsymbol{t}} \cdot \delta \boldsymbol{u} dS = 0. \tag{7}$$

In this framework, the above weak form is discretized by finite elements and the system of discretized equations is solved by the Newmark's algorithm ([25], [26]).

Constitutive model

We consider a perfectly brittle material. The constitutive behavior can be described by the simplest hyperelastic material model, for which

$$\boldsymbol{P} = \frac{\partial W(\boldsymbol{F})}{\partial \boldsymbol{F}}, \tag{8}$$

where $W(\boldsymbol{F})$ is the strain energy density per unit volume. Within a finite time increment in the Newmark's method, the response of the brittle polycrystalline material can be approximated as a small strain problem. In specific, the logarithmic strain is adopted which is defined as [???],

$$\boldsymbol{\varepsilon} = \frac{1}{2} \ln(\boldsymbol{F}^T \boldsymbol{F}). \tag{9}$$

For a high-fidelity prediction of the dynamic response of the materials under extreme loading conditions, such as high pressure and high strain rates, the strain energy density can be divided into the volumetric and isochoric parts,

$$W(\boldsymbol{\varepsilon}) = W^{vol}(J) + W^{iso}(\boldsymbol{\varepsilon}^{iso}). \tag{10}$$

Particularly, the quadratic equation of state and general hook's law are employed to model the volumetric and isochoric responses, respectively, i.e.,

$$W^{vol}(J) = \frac{1}{2} K (J - 1)^2, \tag{11}$$

$$W^{iso}\left(\boldsymbol{\varepsilon}^{iso}\right) = \frac{1}{2} \boldsymbol{\varepsilon}^{iso} : \boldsymbol{C}^{iso} : \boldsymbol{\varepsilon}^{iso}, \tag{12}$$

where K is the bulk modulus and $\boldsymbol{\varepsilon}^{iso}$ is the deviatoric part of the small strain tensor,

$$\boldsymbol{\varepsilon}^{iso} = \boldsymbol{\varepsilon} - \frac{1}{3}\mathrm{tr}(\boldsymbol{\varepsilon})\mathbf{I}\,. \tag{13}$$

Thus, the Cauchy stress tensor $\boldsymbol{\sigma}$ can be derived from Coleman's relations as:

$$\boldsymbol{\sigma} = J^{-1}\boldsymbol{P}\boldsymbol{F}^{T} = K(J-1) + \boldsymbol{C}^{iso}:\boldsymbol{\varepsilon}^{iso}. \tag{14}$$

The constitutive model in the simulations of deformation and failure in brittle materials for a finite size sample is usually homogeneous, and often isotropic. This approximation is fairly adequate as long as the structure has characteristic dimensions much larger than the microstructure dimensions of the materials, i.e. grain sizes. However, this continuum approach breaks down at the microscopic level when dealing with crack initiation and propagation in the microstructure, especially distinguished inter- and transgranular fractures. Indeed, the local stress concentration induced by the microstructure features such as crystal structure and orientations may have a strong influence on the crack growth and eventually affect the ultimate strength of the material. In this framework, the polycrystalline structure is directly simulated and discretized by finite elements. The grain structure is represented by the definition of the grain orientation and misorientation angles at each element. In specific, the grain boundaries consist of elements with non-zero misorientation angles as a transition zone. Figure 1 shows a typical finite element mesh for a polycrystalline structure in 2D.

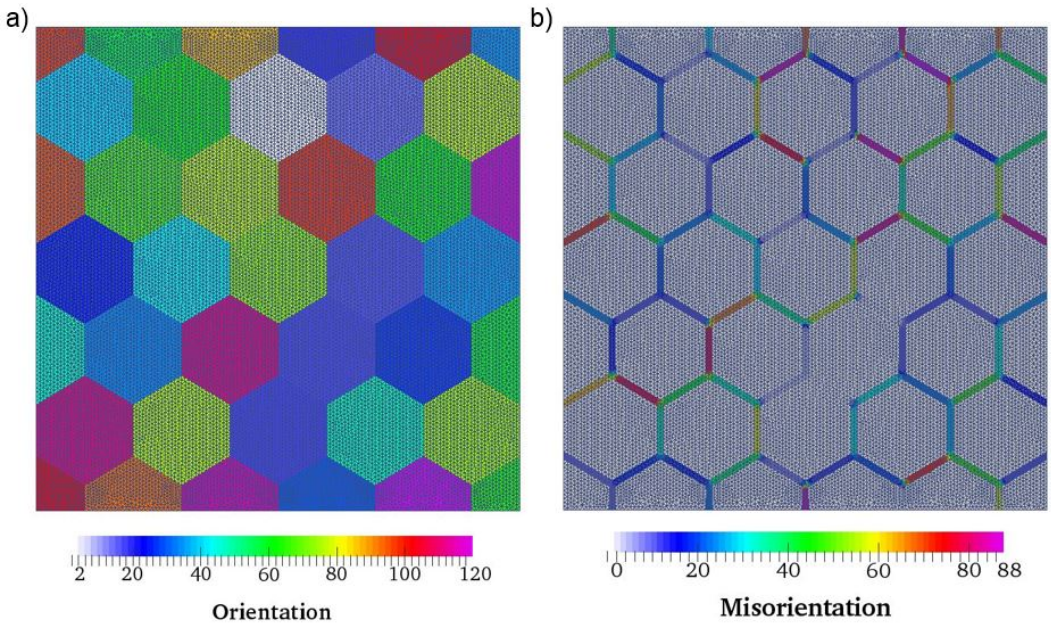

Figure 1. Typical 2D mesh for a polycrystalline structure: a) Grain orientation b) Grain boundary misorientation.

Therefore, a crystallographic constitutive model is employed in the current study to model the anisotropic behavior in the individual grains. The number of independent material parameters in the elastic moduli tensor $\boldsymbol{C}^{iso}$ is subject to the symmetry system of the crystal structure. For the hexagonal structure of SiC, the stiffness tensor can be written in terms of five independent parameters with matrix notation:

$$\boldsymbol{C}=\begin{bmatrix} C_{11} & C_{12} & C_{13} & 0 & 0 & 0 \\ & C_{11} & C_{13} & 0 & 0 & 0 \\ & & C_{33} & 0 & 0 & 0 \\ & & & C_{44} & 0 & 0 \\ & sym & & & C_{44} & 0 \\ & & & & & \frac{C_{11}-C_{12}}{2} \end{bmatrix}. \tag{15}$$

Table 1. The measured elastic constant in a unit of GPa of 6H-SiC at room temperature:

C_{11}	C_{33}	C_{44}	C_{12}	C_{13}
501	553	163	111	52

In order to compute the isochoric stress and strain energy, several elastic constants need to be modified:

$$C_{11}^{iso}=\frac{7C_{11}-2C_{12}-4C_{13}-C_{33}}{9},\ C_{12}^{iso}=\frac{-2C_{11}+7C_{12}-4C_{13}-C_{33}}{9},$$
$$C_{13}^{iso}=\frac{-2C_{11}-2C_{12}+5C_{13}-C_{33}}{9},\ C_{33}^{iso}=\frac{C_{11}+C_{12}+2C_{13}-4C_{33}}{9}. \tag{16}$$

Evaluation of the stresses at each element is performed in the local crystal coordinates instead of the global Cartesian coordinate system. The grain orientation is defined as the angle between the local crystal coordinates and global reference coordinate system, which is denoted by the proper Euler angles (α,β,γ) with respect to rotation axe z-x'-z". In three dimensions, the grain orientations can also be represented by a 3×3 orthonormal rotation matrix $\boldsymbol{R}$, with $\boldsymbol{R}^T\boldsymbol{R}=\mathbf{I}$, i.e.,

$$\boldsymbol{R}=\begin{bmatrix} \cos\alpha\cos\gamma-\cos\beta\sin\alpha\sin\gamma & -\cos\alpha\sin\gamma-\cos\beta\cos\gamma\sin\alpha & \sin\alpha\sin\beta \\ \cos\gamma\sin\alpha+\cos\alpha\cos\beta\sin\gamma & \cos\alpha\cos\beta\cos\gamma-\sin\alpha\sin\gamma & -\cos\alpha\sin\beta \\ \sin\beta\sin\gamma & \cos\gamma\sin\beta & \cos\beta \end{bmatrix}. \tag{17}$$

For non-zero grain orientations, a rotation of the constitutive relation is required. The coordinate transformations of fourth order stiffness tensor can be written in the following tensor notation,

$$C'_{pqrs}=R_{pi}R_{qj}R_{rk}R_{sl}C_{ijkl}, \tag{18}$$

and in the matrix notation as

$$\boldsymbol{C}'=\boldsymbol{D}\boldsymbol{C}\boldsymbol{D}^T, \tag{19}$$

where the 6×6 transformation matrix $\boldsymbol{D}$ related to the $\boldsymbol{R}$ as

$$\boldsymbol{D}=\begin{bmatrix} R_{11}^2 & R_{12}^2 & R_{13}^2 & 2R_{12}R_{13} & 2R_{13}R_{11} & 2R_{11}R_{12} \\ R_{21}^2 & R_{22}^2 & R_{23}^2 & 2R_{22}R_{23} & 2R_{23}R_{21} & 2R_{21}R_{22} \\ R_{31}^2 & R_{32}^2 & R_{33}^2 & 2R_{32}R_{33} & 2R_{33}R_{31} & 2R_{31}R_{32} \\ R_{21}R_{31} & R_{22}R_{32} & R_{23}R_{33} & R_{22}R_{33}+R_{23}R_{32} & R_{21}R_{33}+R_{23}R_{31} & R_{22}R_{31}+R_{21}R_{32} \\ R_{31}R_{11} & R_{32}R_{12} & R_{33}R_{13} & R_{13}R_{32}+R_{12}R_{33} & R_{13}R_{31}+R_{11}R_{33} & R_{11}R_{32}+R_{12}R_{31} \\ R_{11}R_{21} & R_{12}R_{22} & R_{13}R_{23} & R_{12}R_{23}+R_{13}R_{22} & R_{13}R_{21}+R_{11}R_{23} & R_{11}R_{22}+R_{12}R_{21} \end{bmatrix}. \tag{20}$$

Fracture model: Eigen-fracture approach

Finally, we present the Eigen-fracture approach in our framework for tracking the inter- and transgranular fractures in brittle polycrystalline materials. Consider an elastic body occupying a domain $\Omega \subset \mathbb{R}^n$, $n \geq 2$. The boundary of the body consists of an exterior boundary Γ, corresponding to the boundary of the uncracked body, and a collection of cracks jointly defining a crack set $|A|$. To this end, the energy-dissipation functional of a perfectly brittle material is given by

$$F(\boldsymbol{u}, A, t) = \int_{\Omega \setminus A} W\big(\boldsymbol{\varepsilon}(\boldsymbol{u})\big) dV - \int_{\Gamma_t} \bar{\boldsymbol{t}} \cdot \boldsymbol{u} dS + G_c |A|, \tag{21}$$

where Ω\A denotes the domain of the body with the crack set excluded, G_c is the critical energy release rate, and $|A|$ denotes the area of the crack set. Due to the irreversibility of the fracture, the crack set A must be increasing monotonically over time. Thus, the evolution of the crack growth and the corresponding stress field equilibrium can be sought by minimizing $F(\boldsymbol{u}, A, t)$ at all times with respect to both the displacement field $\boldsymbol{u}$ and the crack set A. Nevertheless, a mathematical description of the crack surface is difficult to be derived in engineering applications, especially for three-dimensional problems. With the help of the eigen-deformation field $\boldsymbol{\varepsilon}^*$, which describes the crack set occurring in the material as $\{\boldsymbol{\varepsilon}^* \neq 0\}$, the crack-tracking problem in perfectly brittle materials can be simplified as the minimization of the action [19]

$$F_\epsilon(\boldsymbol{u}, \boldsymbol{\varepsilon}^*, t) = \int_\Omega W(\boldsymbol{\varepsilon}(\boldsymbol{u}) - \boldsymbol{\varepsilon}^*) dV - \int_{\Gamma_t} \bar{\boldsymbol{t}} \cdot \boldsymbol{u} dS + G_c \frac{\|C_\epsilon\|}{2\epsilon}, \tag{22}$$

where ϵ is a small parameter that defines an $\epsilon-$neigborhood of the crack set, B_ϵ, and $||C_\epsilon||$ is the volume of B_ϵ, as shown in Figure 2.

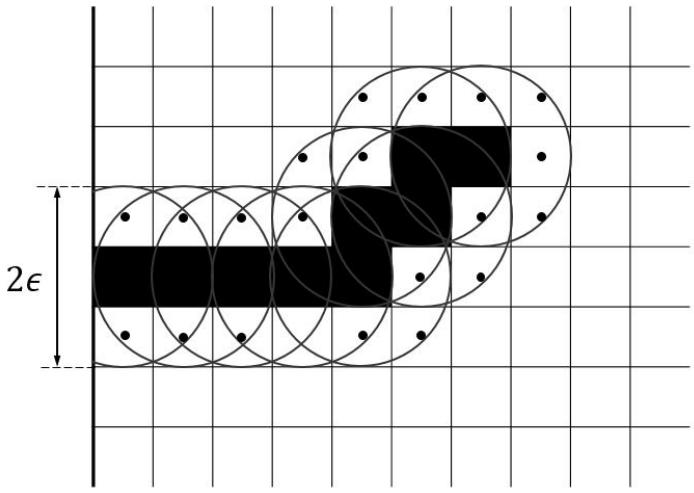

Figure 2.Visulization of the crack ϵ-neighborhood of the crack set $|A|$. Elements in the crack ϵ-neighborhood are marked with black dots.

The stationary of the simplified action in Equation (22) with respect to $\boldsymbol{\varepsilon}^*$ leads to the definition of an effective energy release rate at each finite element, Ω_e, i.e.,

$$G_e = \frac{\alpha\epsilon}{\|C_\epsilon\|} \sum_{\Omega_e \in B_\epsilon} V_e W(\varepsilon). \tag{23}$$

Thus, the energy release rate attendant to the failure of an element is estimated by a local energy averaging procedure in B_ϵ, and elements are failed when the effective energy release rate exceeds the critical energy release rate G_c as a minimizer of $F_\epsilon(\boldsymbol{u}, \boldsymbol{\varepsilon}^*, t)$, i.e., $G_e \geq G_c$. The

calculation of the effective energy release rate is carried out within a local neighborhood of the element and requires no explicit representation of the crack. For linear elasticity, the Eigen-fracture scheme is known to properly converge to the solution of Griffith fracture theory in the limit of vanishingly small mesh sizes [18]. In addition, the local neighborhood averaging of the energy has the effect of eliminating spurious mesh-dependent artifacts. While the minimization problem states the fracture is produced once the averaged local strain energy density exceeds a critical value, it is necessary to further investigate which part of the strain energy density contributes to the crack propagation under complex stress states.[27]. For instance, when an element is under hydrostatic tension, its total strain energy density may be used in the failure criterion to calculate the effective energy release rate. But when an element is under hydrostatic compression, only the isochoric strain energy is dissipated due to new fracture surface generation.

On the other hand, in the Griffith theory of brittle fracture, the critical energy release rate can be related to the surface energy density of potential fracture surfaces. It has been generally recognized that the fracture resistance of brittle materials heavily relies on the distribution of topological defects in the microstructure including grain boundaries, porosity and second phase particles, under dynamic loading conditions. In another word, the surface energy density is no longer a single value for a specific type of material but should be considered as a function of the local microstructure features. Consequently, by integrating a microstructure-informed critical energy release rate in the Eigen-fracture approach at each element, it allows us to explicitly model the interactions between the fracture and topological defects in the microstructure. In this work, only the grain boundaries are explicitly accounted for, where the critical energy release rate can be written as $G_c^{gb} = 2\gamma_{gb}$, with γ_{gb} the surface energy density of the grain boundary or grain boundary energy. In Reed and Shockley's dislocation model [28], a simple formula of grain boundary energy is derived for a 2-D cubic elastic material with small misorientation angles $\theta < 45^{\circ}$. In this formula, the grain boundary energy increases as the misorientation angle increases. However, in reality, the grain boundary properties such as energy, mobility, and diffusivity etc. are much more complicated, especially for a 3-D problem. Abrupt changes or even discontinuity may occur at critical misorientation angles. Therefore, in this work, G_c^{gb} is defined in Equation (24) as a power law function of its misorientation angle for the sake of simplicity. A more precise study will be deployed in the future using MD simulations.

$$G_c(\theta) = G_{c0}\left[1 - \left(\frac{\theta}{\theta_0}\right)^m\right], \tag{24}$$

where G_{c0} is the critical energy release rate of a single crystal, θ_0 is the reference misorientation angle, m is the exponential for grain boundary weakening. The misorientation angle θ can be calculated using the orientations of two neighboring grains,

$$\theta = \min\left|\cos^{-1}\left\{\frac{tr(\boldsymbol{R}_B\boldsymbol{R}_A^{-1})-1}{2}\right\}\right|. \tag{25}$$

where $\boldsymbol{R}_A$ and $\boldsymbol{R}_B$ are the rotation matrices for two neighboring grains A and B.

Numerical Simulations and Results

The proposed micromechanical computational framework is utilized to understand the rate dependence of the compressive strength of brittle polycrystalline materials. Particularly, the dynamic response of 6H-SiC under compressive loading in split Hopkins pressure bar experiments[29] is studied numerically in this work.

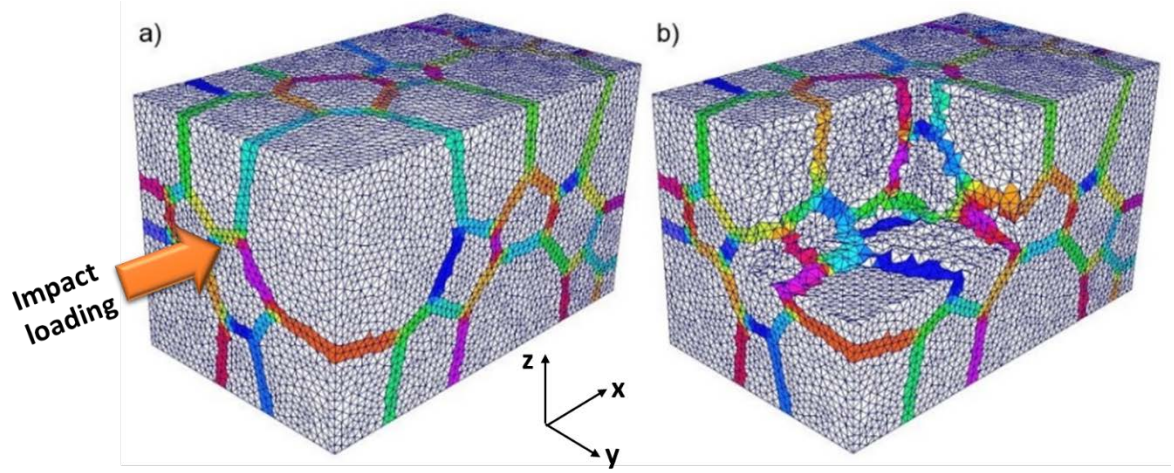

Figure 3. a) Surface meshes of the specimen and b) Interior meshes: Inner grain elements (grey) is enclosed by grain boundary elements (colored). Note that the color denotes the misorientation angles.

Figure 3 shows a typical 3D mesh of the polycrystalline brittle material in our simulations. The boundary conditions are illustrated in Figure 3 (a). The nodes on the front surface are assigned with displacements in x-direction following a linearly increasing velocity up to a constant value, while the nodes on the back surface can only move in y-z plane. The polycrystalline specimen consists of 45 equiaxed grains, which aggregate a cuboid with a dimension of 1000 μm × 600 μm × 600 μm. The average volume for an individual grain, V_{grain} is about 8×10^6 μm^3. The average grain size can be estimated as $d = \sqrt[3]{V_{grain}} = 200\,\mu m$. The computational mesh comprises 76,142 nodes and 427,264 tetrahedra. The grain boundaries are represented by two thin layers of elements adjacent to the interior surfaces. All the meshes on the interior surfaces are conformal and their nodes are shared by neighboring grain boundary elements. The average volume ratio between grain boundary and inter-grain elements is about 29.5%. The material properties and model parameters used in the simulations are listed in Table 2.

Table 2. Parameters used in simulation

Parameter	Value	Definition
K	231	Bulk modulus [GPa]
μ	192	Shear modulus [GPa]
ρ	3.21	Density [g/cm^3]
ν	0.16	Poisson's ratio
G_c	50	Critical energy release rate for single crystal [J/m^2]
θ_0	180	Relative misorientation angle in G_c^{gb} function [degree]
m	0.5	Exponential for grain boundary weakening
ϵ	$1.5h_e$	Epsilon neighbor size, where h_e is the element size

A series of snapshots in Figure 4 illustrates the fracture evolution at strain rate 3300 s^{-1}. The black translucent structure denotes the grain boundaries while the reddish elements represent the fracture zone. As shown in Figure 4(a), the cracks first initiate at grain boundaries on the front and back surfaces of the specimen. As the stress increases, weak grain boundaries inside of the specimen start to fail. While the intergranular cracks propagate into the material, the transition from intergranular fracture to transgranular fracture occurs as demonstrated in Figure

4(b). The transgranular fracture grows along the loading direction and creates longitudinal splits on the peripheral surfaces in Figure 4(c), which agrees well with the experimental observations [2]. The transgranular fractures connect the spatially dispersed grain boundary cracks into a network. As a result, the initially integrated material are divided into several pillars. In the end, the divided material comminutes one by one very rapidly until all the material fails as the deposited energy accumulates, Figure 4(d).

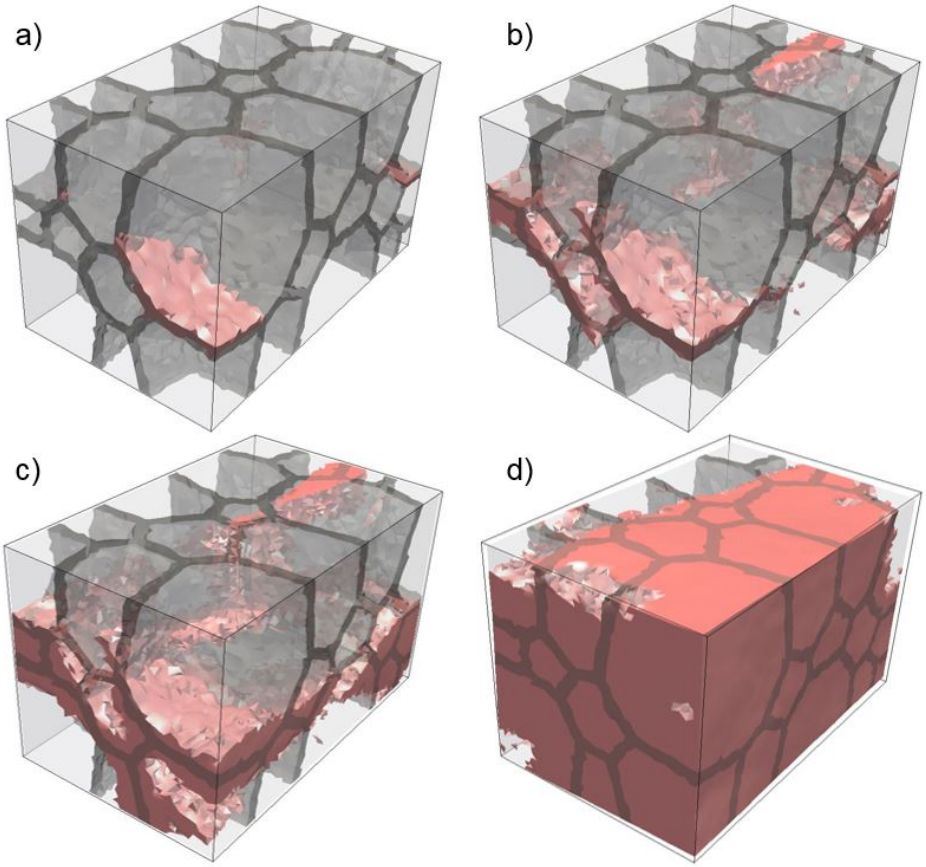

Figure 4. Evolution for cracks under uniaxial compression: a) crack surfaces initiation at grain boundaries, b) crack propagation, c) interaction between cracks and d) comminution.

The corresponding stress history of SiC under compressive loading at strain rate 3300 s^{-1} is shown in Figure 5. The stress is calculated as the homogenized one over the entire specimen alone the loading axis. As seen in the figure, the predicted compressive strength of SiC at strain rate 3300 s^{-1} by the direct numerical simulation of the polycrystalline structure is 3.45 GPa. After the stress reaches the peak, it dramatically drops and then becomes stable. The residual stress after the drop is due to the resistance to deformation in the comminuted material. Comparing Figure 4 to Figure 5, it is interesting to note that the stress continues to build up after the initial grain boundary cracks. The strengthening gradually slows down as the transgranular fracture propagates. When individual cracks coalesce with each other into a network, the stress approaches its maximum level. Afterward, the stress suffers a sudden decrease due to the material comminution.

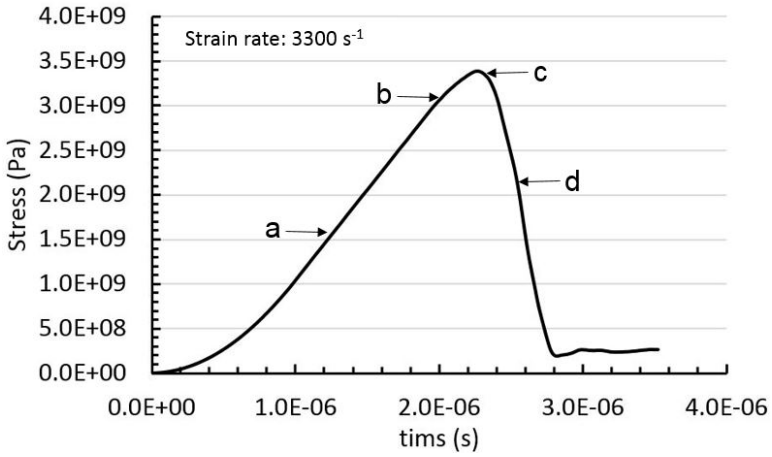

Figure 5. Stress history for strain rate at 3300 s^{-1}. The "a", "b", "c" and "d" locations pointed out in the stress curve correspond with the series of fracture images shown in Figure 4.

The same mesh and material configuration were exercised under dynamic compressive loading conditions at five different strain rates, ranging from O(10) to O(10^4) s^{-1}. The compressive strengths at various strain rates are plotted in Figure 6. The nonlinearity of strain rate dependence is illustrated in the figure. It is evident that there is a critical turning point between the strain rate 100 s^{-1} and 1000 s^{-1}. Before the turning point, the compressive strength increases slightly as the strain rate increases. As the strain rate goes beyond 1000 s^{-1}, a dramatic jump in the compressive strength is developed. The critical turning point predicted by our model matches well with the experimental measurements by Sarva and Nasser[1]. It is worth mentioning that neither the constitutive model nor the fracture model is defined to be rate dependent in our framework. The strain rate dependence of the compressive strength is a natural output of the model and results from the selection of the most effective energy dissipation pathways (i.e. intergranular or transgranular fracture) in the microstructure automatically by the algorithm. Therefore, the micromechanical computational framework allows us to develop a fundamental understanding of the rate-dependent fracture properties without introducing rate-dependent material parameters that need to be calibrated to experiments.

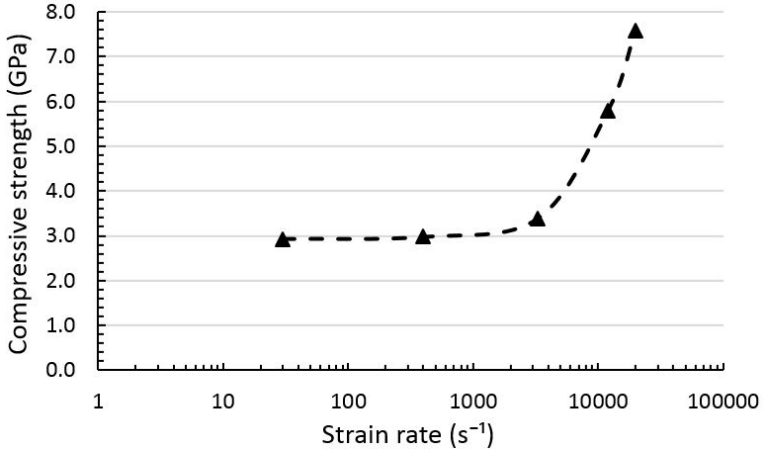

Figure 6. Strain rate dependent compressive strength of polycrystalline SiC predicted by the model.

Conclusions and Future Work

We have developed a three-dimensional micromechanical computational framework for the direct numerical simulation (DNS) of failure in brittle polycrystalline structures based on the finite element method and Eigen-fracture approach. The interaction of crack with the topological defects, such as grain boundaries, in the microstructure is explicitly modeled by considering the equivalent energy release rate as a function of the microstructural features, in specific, the grain boundary misorientation angles. The anisotropic dynamic response of polycrystalline structures is predicted by using the crystal elasticity model with local material properties related to the grain orientation and misorientations. The numerical model is validated in the example of unconfined dynamic compression tests of 6H-SiC at different strain rates. Without introducing any rate-dependent model parameters, the computational framework successfully predicts the rate sensitivity in the compressive strength of brittle polycrystalline structures. Our results show the rate dependence is intimately related to the competition and combination of intergranular and transgranular fractures in the microstructure. The selection of the optimal energy dissipation pathways in the microstructure in the case of high energy density deposition in a short time determines the ultimate strength of the brittle polycrystalline materials. It is evident that the proposed computational framework enables an automatic selection of the most effective energy dissipation pathways by integrating topological defect dependent local energy release rates in the DNS of the polycrystalline microstructure. Further investigation is necessary in order to quantify the correlation between the dynamic strength and the comparison of trans- and intergranular fractures at the microscale.

References

[1] S. Sarva and S. Nemat-nasser, “Dynamic compressive strength of silicon carbide under uniaxial compression,” vol. 317, pp. 140–144, 2001.

[2] H. Wang and K. T. Ramesh, “Dynamic strength and fragmentation of hot-pressed silicon carbide under uniaxial compression,” *Acta Mater.*, vol. 52, no. 2, pp. 355–367, 2004.

[3] G. Hu, C. Q. Chen, K. T. Ramesh, and J. W. Mccauley, “Mechanisms of Dynamic Deformation and Dynamic Failure in Aluminum Nitride,” vol. 60, no. June, pp. 3480–3490, 2012.

[4] G. Hu, K. T. Ramesh, B. Cao, and J. W. Mccauley, “The Compressive Failure of Aluminum Nitride Considered as a Model Advanced Ceramic,” vol. 59, no. June, pp. 1076–1093, 2012.

[5] W. Chen and G. Ravichandran, “Failure mode transition in ceramics under dynamic multiaxial compression,” *Int. J. Fract.*, vol. 101, no. 1–2, pp. 141–159, 2000.

[6] S. Nemat-Nasser and H. Deng, “Strain-rate effect on brittle failure in compression,” *Acta Metall. Mater.*, vol. 42, no. 3, pp. 1013–1024, 1994.

[7] H. D. Espinosa and P. D. Zavattieri, *A grain level model for the study of failure initiation and evolution in polycrystalline brittle materials. Part I: Theory and numerical implementation*, vol. 35, no. 3–6. 2003.

[8] S. Maiti, K. Rangaswamy, and P. H. Geubelle, “Mesoscale analysis of dynamic fragmentation of ceramics under tension,” *Acta Mater.*, vol. 53, no. 3, pp. 823–834, 2005.

[9] P. G. Nittur, S. Maiti, and P. H. Geubelle, “Grain-level analysis of dynamic fragmentation of ceramics under multi-axial compression,” *J. Mech. Phys. Solids*, vol. 56, no. 3, pp. 993–1017, 2008.

[10] G. K. Sfantos and M. H. Aliabadi, “Aboundary cohesive grain element formulation formodelling intergranularmicrofracture in polycrystalline brittle,” no. July 2006, pp. 1590–1626, 2012.

[11] G. Ruiz, M. Ortiz, and A. Pandolÿ, “Three-dimensional ÿnite-element simulation of the dynamic Brazilian tests on concrete cylinders,” no. January 1999, pp. 963–994, 2000.

[12] G. T. Camacho and M. Ortiz, “Computational modelling of impact damage in brittle materials,” *Int. J. Solids Struct.*, vol. 33, no. 20–22, pp. 2899–2938, 1996.

[13] M. Negri, “Numerische Mathematik A finite element approximation of the Griffith ’ s model,” pp. 653–687, 2003.

[14] C. M. Landis, “A phase-field description of dynamic brittle fracture by,” no. May, 2011.

[15] J. D. C. J. Knap, “A geometrically nonlinear phase field theory of brittle fracture,” pp. 139–148, 2014.

[16] J. D. Clayton and J. Knap, “Phase field modeling of directional fracture in anisotropic polycrystals,” *Comput. Mater. Sci.*, vol. 98, no. February, pp. 158–169, 2015.

[17] B. Bourdin, G. A. Francfort, and J. Marigo, *The Variational Approach to Fracture*. 2008.

[18] B. Schmidt, F. Fraternali, and M. Ortiz, “Eigenfracture: an eigendeformation approach to variational

fracture ∗," vol. 7, no. 3, pp. 1237–1266, 2009.
[19] A. Pandolfi and M. Ortiz, "An eigenerosion approach to brittle fracture," *Int. J. Numer. Methods Eng.*, vol. 92, no. 8, pp. 694–714, 2012.
[20] C. J. Larsen, M. Ortiz, and C. L. Richardson, "Fracture Paths from Front Kinetics : Relaxation and Rate Independence," vol. 193, pp. 539–583, 2009.
[21] A. Mielke and M. Ortiz, "A CLASS OF MINIMUM PRINCIPLES FOR CHARACTERIZING THE TRAJECTORIES AND THE RELAXATION OF DISSIPATIVE SYSTEMS," vol. 14, pp. 494–516, 2008.
[22] J. M. J. Den Toonder, J. a W. Van Dommelen, and F. P. T. Baaijens, "The relation between single crystal elasticity and the effective elastic behaviour of polycrystalline materials: theory, measurement and computation," *Model. Simul. Mater. Sci. Eng.*, vol. 7, no. 6, pp. 909–928, 2000.
[23] A. Fallahi, A. Ataee, G. Tial, and C. Stresses, "Effects of Crystal Orientation on Stress Distribution Near the Triple Junction in a Tricrystal γ -TiAl," *Mater. Sci. Technol.*, pp. 1–13, 2008.
[24] B. Li, A. Pandolfi, and M. Ortiz, "Mechanics of Materials Material-point erosion simulation of dynamic fragmentation of metals," 2014.
[25] T. Belytschko, "An overview of semidiscretization and time integration procedures," in *Computational Methods for Transient Analysis*, North-Holland, Amsterdam, 1983, pp. 1–65.
[26] T. J. R. Hughes, "Analysis of transient algorithms with particular reference to stability behavior," in *Computational Methods for Transient Analysis*, North-Holland, Amsterdam, 1983, pp. 67–155.
[27] Q. M. Li, "Strain energy density failure criterion," vol. 38, pp. 6997–7013, 2001.
[28] W. T. R. W.Shockley, "Dislocation Models of Crystal Grain Boundary," *Phys. Rev.*, vol. 78, no. 3, pp. 275–289, 1950.
[29] K. T. Ramesh, "High Strain R 33.1," *Handb. Exp. Solid Mech.*, p. 874, 2008.